Phys. Med. Biol. **45** (2000) 1495–1509. Printed in the UK PII: S0031-9155(00)07527-8

Non-invasive quantitative reconstruction of tissue elasticity using an iterative forward approach

D Fu†, S F Levinson†‡, S M Gracewski§ and K J Parker†

† Department of Electrical and Computer Engineering, University of Rochester, Rochester, NY 14627, USA

‡ Department of Physical Medicine and Rehabilitation, University of Rochester, Rochester, NY 14627, USA

§ Department of Mechanical Engineering, University of Rochester, Rochester, NY 14627, USA

Received 7 September 1999, in final form 4 January 2000

Abstract. A novel iterative approach is presented to estimate Young's modulus in homogeneous soft tissues using vibration sonoelastography. A low-frequency (below 100 Hz) external vibration is applied and three or more consecutive frames of B-scan image data are recorded. The internal vibrational motion of the soft tissue structures is calculated from 2D displacements between pairs of consecutive frames, which are estimated using a mesh-based speckle tracking method. An iterative forward finite element approach has been developed to reconstruct Young's modulus from the measured vibrational motion. This is accomplished by subdividing the 2D image domain into sample blocks in which Young's modulus is assumed to be constant. Because the finite element equations are internally consistent, boundary values other than displacement are not required. The sensitivity of the results to Poisson's ratio and the damping coefficient (viscosity) is investigated. The approach is verified using simulated displacement data and using data from tissue-mimicking phantoms.

1. Introduction

Soft tissue elasticity imaging holds great promise because Young's modulus is known to be affected by tissue pathology or, in the case of muscle contraction, by physiological processes. However, no method exists for the quantitative reconstruction of elastic properties. As the equations of motion may involve second- and even third-order spatial derivatives that can dramatically increase sensitivity to noise, most approaches have either been qualitative or have used simplified, but limited, models. A robust method for elastic modulus reconstruction could significantly advance imaging capabilities.

The earliest reported approach involved vibration sonoelastography (elastography based on ultrasonic imaging of forced tissue vibration) with a simplified model of vibration decay that was not readily adapted to imaging (Krouskop *et al* 1987). A variation of this approach made use of the phase gradient of the Doppler signal to estimate vibration wave speed, which is related to Young's modulus if a plane wave model is assumed (Yamakoshi *et al* 1990). This was subsequently adapted by Levinson *et al* (1995) to measure changes in muscle elastic properties with contraction. An alternative qualitative approach made use of the variance of the Doppler signal to image malignant tumours, which tend to be relatively hard compared with surrounding tissues (Lerner *et al* 1990, Parker *et al* 1990, 1998, Gao *et al* 1995). Other approaches to vibration elastography have included magnetic resonance elastography (Muthupillai *et al* 1995), which suffers from a very low frame rate, and an acoustic impulse technique (Catheline *et al* 1999) that requires the use of ultrafast ultrasonic imaging techniques.

0031-9155/00/061495+15$30.00

Methods involving static tissue compression have received particular attention of late due to their inherent simplicity. Commonly, the issue of elastic reconstruction is side-stepped by assuming that variations in tissue strain are qualitatively representative of variations in elastic properties. This approach has been used successfully to image relative elastic properties in the detection of otherwise isoechoic lesions in both tissue-mimicking phantoms and in human tissues (Ophir *et al* 1991, 1997, O'Donnell *et al* 1994, Skovoroda *et al* 1995). The primary disadvantage is that artefacts often result because strain is not uniquely determined by variations in Young's modulus, but also by tissue geometry and the distribution of applied forces.

Quantitative reconstruction of soft tissue viscoelastic properties remains the most problematic aspect of virtually all methods of elastography. Skovoroda *et al* (1995) presented a general approach to elastic reconstruction for a linear, elastic, isotropic, incompressible medium subjected to external static compression, based on a plane strain model and known boundary conditions. Skovoroda *et al* (1999) also investigated the problem for large deformations, in which nonlinear displacement–strain relations with high-order spatial derivatives are used. Kallel and Bertrand (1996) developed a regularized linear perturbation approach based on a finite element model and Tikhonov regularization theory. Sumi *et al* (1995) proposed a solution to the inverse problem based on a plane stress model from which two-dimensional equilibrium equations are derived, and the spatial distribution of the relative shear modulus is obtained by integration. Romano *et al* (1998) presented the theory and a numerical simulation for non-invasive determination of the material parameter ratios for isotropic, linear elastic media subjected to harmonic vibration.

In this paper, we present a novel iterative forward approach to quantitative estimation of Young's modulus in vibration sonoelastography. In our implementation, three or more consecutive frames of B-scan data are recorded. The two-dimensional displacements between each pair of consecutive frames are estimated using a mesh-based speckle tracking method in which only estimates obtained from nodes with a high feature energy are used, minimizing the risk of speckle decorrelation. The amplitude and phase of the vibration motion vectors are calculated from the estimated displacements. Elastic property reconstruction is formulated as a forward problem based on finite element theory in which an arbitrary region of interest (ROI) is chosen for which Young's modulus, Poisson's ratio and the damping coefficient (viscosity) are assumed to be constant. Given the measured amplitude and phase values of displacement along the boundary of the ROI, the motion vectors for the internal nodes can be calculated from finite element theory based on assumed values of the viscoelastic parameters. An error estimate, calculated from the sum-squared difference (ssd) between the predicted motions and the measured data, is then used to refine the estimate of one or more of these parameters and the procedure is repeated until the minimum ssd is obtained. Because both ultrasonic tissue motion estimation and elastic property reconstruction are mesh-based, their integration through the use of the same mesh structure for both provides a systems approach by which the mechanical properties can be derived from vibrating ultrasonic image sequences. The approach has been tested on both synthetic data and experimental data from tissue-mimicking phantoms.

2. Theory

2.1. Mechanical model of tissue dynamics

The force equilibrium equations that govern the dynamic response of a medium can be expressed as

$$\sigma_{ij,j} + \rho f_i = \rho \frac{\partial^2 u_i}{\partial t^2} \qquad (i = 1, 2, 3) \tag{1}$$

where σ_{ij} is the stress tensor, f_i is the body force vector, u_i is the displacement vector in Cartesian coordinates x_i, ρ is the mass density of the medium; commas in the subscript denote partial differentiation with respect to the indices that follow and summation over repeated indices is implied.

If the material is assumed to be linear, homogeneous, isotropic and viscoelastic, the Voigt model can be used to establish the constitutive equations

$$\sigma_{ij} = \left(\lambda_1 + \lambda_2 \frac{\partial}{\partial t}\right)\epsilon_{kk}\delta_{ij} + 2\left(\mu_1 + \mu_2 \frac{\partial}{\partial t}\right)\epsilon_{ij} \tag{2}$$

where δ_{ij} is the Kronecker delta and ϵ_{ij} is the strain tensor, given by

$$\epsilon_{ij} = (u_{i,j} + u_{j,i})/2 \tag{3}$$

for small displacements. λ_1 and μ_1 are the longitudinal and shear elastic modulus respectively, and λ_2 and μ_2 are the longitudinal and shear viscous modulus respectively. λ_1 and μ_1 are also called Lamé parameters, which are related to Young's modulus and Poisson's ratio through the expressions

$$\lambda_1 = \frac{E\nu}{(1+\nu)(1-2\nu)} \qquad \mu_1 = \frac{E}{2(1+\nu)}. \tag{4}$$

The damping coefficient, which relates the viscous modulus to the elastic modulus, is defined as $\xi = \omega\lambda_2/\lambda_1 = \omega\mu_2/\mu_1$ where ω is the angular frequency of the vibration. Thus, given the values of E, ν and ξ, all of the elastic and viscous moduli in equation (2) can be determined. Substituting equations (2) and (3) into equation (1) yields the governing equations for a dynamic medium

$$\left(\mu_1 + \mu_2 \frac{\partial}{\partial t}\right)u_{i,jj} + \left((\mu_1 + \lambda_1) + (\mu_2 + \lambda_2)\frac{\partial}{\partial t}\right)u_{j,ji} = \rho \frac{\partial^2 u_i}{\partial t^2}. \tag{5}$$

Because most current ultrasound scanners can acquire only two-dimensional information, a plane strain limitation is introduced to establish a 2D mechanical model. The plane strain problem is defined as a deformation state in which $u_3 = 0$ everywhere and u_1 and u_2 are functions of x_1 and x_2 but not of x_3. As such, $u_1 = u_1(x_1, x_2)$ and $u_2 = u_2(x_1, x_2)$.

In reality, tissue objects are three dimensional. However, in some applications, specific body geometry and loading patterns can lead to a reduced, essentially two-dimensional, problem. For example, in the human body the plane strain situation can be approximated by uniform loading of essentially cylindrical objects such as the limbs. The mechanical model used in this paper, shown in figure 1, is a three-dimensional object. The geometry of cross sections and the applied vibration source are uniform along the longitudinal dimension, which is much larger than the other two directional dimensions. The vibration displacements in the slices near the middle of the object approximately satisfy the conditions required for the plane strain problem and can be analysed using plane strain theory.

2.2. Iterative solution to elasticity

The finite element method (FEM), which uses a numerical procedure to obtain a discrete approximation in both static and dynamic problems, is well suited to the solution of the governing equation in equation (5). Equations that govern the dynamic response of a medium are derived by requiring the work of the external vibration forces to be absorbed by the work of internal, inertial and viscous forces for small admissible motions. For a single element, the equilibrium equation for the harmonic vibration case is expressed as (Cook *et al* 1989)

$$(-\omega^2[m] + \mathrm{i}\omega[c] + [k])\{d\} = \{r\} \tag{6}$$

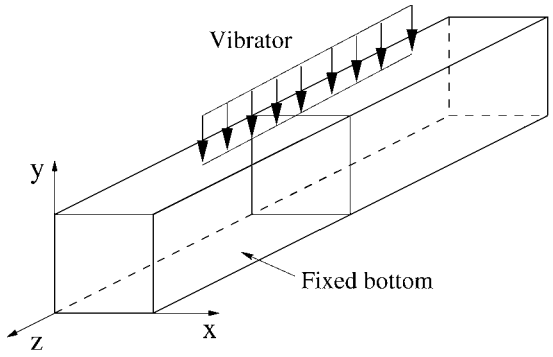

Figure 1. Mechanical model in which a cross section near the middle of the object approximates a plane strain state.

where $[m]$, $[c]$ and $[k]$ are the element mass, damping and stiffness matrices respectively, $\{d\}$ and $\{r\}$ are the element grid displacement and force vectors respectively, ω is the angular frequency of vibration and i is the imaginary unit. The $[m]$, $[c]$ and $[k]$ matrices depend on ρ, (λ_2, μ_2), and (λ_1, μ_1) respectively. After assembly of elements, the governing equations in FEM are derived from equation (6)

$$(-\omega^2[M] + \mathrm{i}\omega[C] + [K])\{D\} = \{R\} \tag{7}$$

where $[M]$, $[C]$ and $[K]$ are the assembled element mass, damping and stiffness matrices respectively and $\{D\}$ and $\{R\}$ are the assembled element grid displacement and force vectors respectively.

In the case of harmonic vibration, the grid displacement and force are expressed as

$$D = A\,\mathrm{e}^{\mathrm{i}(\omega t+\theta)} \qquad R = B\,\mathrm{e}^{\mathrm{i}(\omega t+\phi)} \tag{8}$$

where A and θ are the displacement amplitude and phase vectors respectively, and B and ϕ are the force amplitude and phase vectors respectively. After substituting equation (8) into equation (7), the governing equations in the frequency domain can be obtained as

$$\begin{bmatrix} -\omega^2 M + K & -\omega C \\ \omega C & -\omega^2 M + K \end{bmatrix} \begin{Bmatrix} A\cos\theta \\ A\sin\theta \end{Bmatrix} = \begin{Bmatrix} B\cos\phi \\ B\sin\phi \end{Bmatrix}. \tag{9}$$

The vibration displacement amplitude and phase can be obtained by solving equation (9), given the object geometry, the boundary constraints, the forcing conditions and the mechanical properties of the material at every point. Figure 2 shows a two-dimensional mesh representation of a slice of the object shown in figure 1. An arbitrary region of interest (ROI) is chosen for consideration. If the displacement amplitude and phase are known for all points along the boundary of the ROI, the force terms can be eliminated by simple matrix manipulation of equation (9) and the displacements of all internal points can be uniquely determined.

The goal in the reconstruction of soft tissue elastic properties is to estimate values of Young's modulus from the measured vibration amplitude and phase values. Although Poisson's ratio and the damping coefficient are also unknown, for the purposes of this paper they will be assumed to be constant. Values of Poisson's ratio should fall between 0 and 0.5, with $\nu = 0.5$ for an incompressible material. Although soft tissues are often considered to be incompressible, as $\nu \to 0.5$, equation (4) becomes unstable because of the $1 - 2\nu$ term in the denominator of λ_1. Poisson's ratio is often set arbitrarily to a value of 0.495 (e.g. Parker *et al* 1990), representing a 1% deviation from incompressibility. Although values closer to 0.5 may be more realistic, the instability in equation (4) becomes more of an issue. We have chosen to

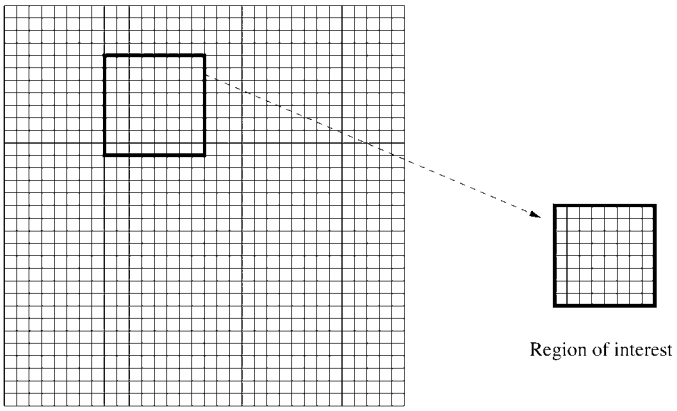

Figure 2. 2D mesh representation of a cross section in which the block shown is an arbitrary region of interest (ROI) within which the mechanical properties are assumed to be constant.

use $\nu = 0.495$, and will explore the validity of this assumption using a numerical simulation in the next section.

Unfortunately, only limited data are available on the viscosity of soft tissues. Based on our own measurements of stress/strain relationships in soft tissue phantoms, we have chosen to ignore damping for the time being. Under conditions where ωC is very small compared with $-\omega^2 M + K$, damping can indeed be ignored and equation (9) can be simplified to

$$[-\omega^2 M + K]\{A\cos\theta\} = \{B\cos\theta\}. \tag{10}$$

The effect of assuming the undamped condition will be investigated in the next section.

The basic principle behind the iterative approach is as follows: given an assumed Young's modulus, solution of equation (10) will result in theoretical estimates of the vibration displacements. These are then compared with the measured data and Young's modulus is iteratively updated until convergence within a specified constraint is achieved. The range of Young's modulus values is given by $E_{\min} < E_e < E_{\max}$, where $E_{\min}$ and $E_{\max}$ are the minimum and maximum expected values, and E_e is the estimated value. Typically, Young's modulus for living soft tissue ranges from 1 kPa to 200 kPa for strains of less than 5% (Radmacher 1997, Levinson *et al* 1995, Krouskop *et al* 1998). Defining $\Delta A = \sum(A_e - A_m)$, ssd $= \sum(A_e - A_m)^2$ and $\Delta E = E_{\max} - E_{\min}$, where A_e and A_m are the estimated and the measured amplitude respectively, the steps of implementation are as follows:

1. Initialize values of $E_{\min}$ and $E_{\max}$.
2. Assume an estimated Young's modulus $E_e = (E_{\min} + E_{\max})/2$.
3. Solve equation (10) for amplitude, A_e, and calculate ΔA.
4. Update $E_{\min}$ and $E_{\max}$ in the following way:
   (a) If $\Delta A > 0$, then set $E_{\min} = E_e$ and keep $E_{\max}$.
   (b) If $\Delta A < 0$, then set $E_{\max} = E_e$ and keep $E_{\min}$.
5. Repeat steps 2, 3 and 4 until $\Delta E/E_e <$ threshold or until M iterations.

The threshold may be set to any value less than half the expected error and the maximum iteration number, M, is arbitrary. For the purposes of our work, the threshold was set to 2% and M to 13.

2.3. Estimation of amplitude and phase

Solving for Young's modulus using the iterative forward approach requires complete 2D vibration amplitude and phase vector field information. Yeung *et al* (1998) developed a mesh-based speckle tracking method based on approaches that are often used in video coding, but adapted for ultrasonic motion tracking. The method employs an adaptive deformable mesh that makes use of image feature energy for assignment of mesh nodes. Ultrasonic speckle results from the constructive and destructive interference of coherent acoustic waves impinging on the ultrasonic transducer. Feature energy is calculated using a steerable wavelet transform of the image to select speckle patterns that are likely to be stable. A finite element method is then used to manipulate the resulting irregular mesh. In order to track both large and small deformations, a hierarchical scheme is used in which estimates are obtained for a coarse mesh first, which is successively divided into finer mesh elements with each successive level of the algorithm.

Amplitude and phase information can be uniquely recovered, in theory, using as few as three consecutive image frames. A consecutive ultrasound image sequence with N frames is assumed. Using the first frame as the reference frame, the displacement in the x_i direction between frames 1 and n, $\delta u_{i(n)}(x_1, x_2)$ can be estimated using the mesh-based speckle tracking method.

The displacement at the point (x_1, x_2) at time t can expressed as

$$u_i(x_1, x_2, t) = A_i(x_1, x_2)\cos(2\pi f t + \theta_i(x_1, x_2)) \qquad (i = 1, 2) \tag{11}$$

where $A_i(x_1, x_2)$ and $\theta_i(x_1, x_2)$ are the amplitude and phase at the point (x_1, x_2) in the x_i direction. If the vibration frequency f and the frame rate f_s are chosen so that $f = (I \pm 1/4) f_s$, where I is an arbitrary integer, the displacements between any two consecutive frames can be maximized. Because the maximum frame rate for B-scan images in our system is usually 30 Hz, the vibration frequencies chosen in our implementation were 22.5 Hz, 37.5 Hz, 52.5 Hz, 67.5 Hz and so on. The relationship between the vibration motion (amplitude and phase) and the displacements between frame n and frame 1 is:

$$\delta u_{i(n)}/A_i = \cos(2\pi(n-1)f/f_s + \theta_i) - \cos(\theta_i) \qquad (i = 1, 2). \tag{12}$$

The equations are over-constrained when $N > 3$. In this case, the least squared error can be minimized to obtain estimates of the amplitude A_i and the phase ϕ_i.

3. Numerical simulation

Validation of our approach requires demonstration of its accuracy, the ability to detect regional differences in elasticity and relative immunity to noise. As a first approach to the evaluation of accuracy and the ability to handle spatial variation, we have developed an FEM simulation of a two-layer structure in which one layer is twice as hard as the second. The amplitude and phase response of a mechanical 3D model, shown in figure 1, to a hypothetical applied vibration is solved using MSC/NASTRAN (MacNeal-Schwendler Corporation, Los Angeles, CA), a commercial FEM package. Motion information is extracted from the central cross section, shown in figure 3. The extracted 2D motion field is then used to simulate tissue displacements for use in solving for Young's modulus with the iterative forward approach.

The choice of the mechanical parameters for the MSC/NASTRAN FEM simulation is arbitrary, but should be realistic and comparable with the actual properties of the tissues to be studied. Young's modulus is typically between 1 kPa and 200 kPa in biological soft tissues (Parker *et al* 1990, Radmacher 1997, Krouskop *et al* 1998). We chose $E_1 = 20$ kPa and $E_2 = 10$ kPa.

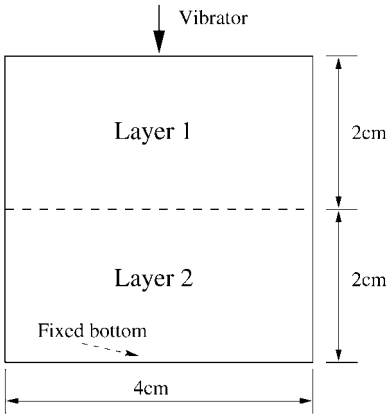

Figure 3. Diagram of a slice in a two-layer structure in which the two layers have differing Young's moduli.

Although specific data on Poisson's ratio are difficult to find, values can be deduced from known acoustic properties. It is well known that the longitudinal sound speed is about $v_l = 1540$ m s^{-1}. From this and from the range of Young's moduli, it is calculated that the shear sound speed, v_s, should range from 1 m s^{-1} to 8 m s^{-1} so long as the strain is less than 5%. For plane wave propagation in unbounded media, the sound speeds v_l and v_s can be expressed as

$$v_l = \sqrt{\frac{\lambda_1 + 2\mu_1}{\rho}} \qquad v_s = \sqrt{\frac{\mu_1}{\rho}} \tag{13}$$

from which Poisson's ratio can be formulated as

$$\nu = \frac{v_l^2 - 2v_s^2}{2v_l^2 + 2v_s^2}. \tag{14}$$

The range of Poisson's ratio is thus predicted to be approximately from 0.499 96 to 0.499 9995. We chose a value of $\nu_1 = \nu_2 = 0.499\,995$, which is within the expected range.

Because few data are available on the damping coefficients of living soft tissues, an arbitrary small damping value was assumed for the purposes of simulation. Based on data obtained from a simple experiment involving the measurement of stress and strain under forced vibration, using a small sample of the material used for our gel-based phantoms as described in the next section, we set $\xi_1 = \xi_2 = 0.05$.

As a test of convergence, a vibration frequency $f = 37.5$ Hz was used in the simulation and equation (9) was used in the iterative forward estimation algorithm with the exact parameters of ν and ξ that were used to generate the simulated data. Two arbitrary regions of interest were chosen in the soft and hard layers respectively. Because the ideal data are noise-free, the size of the ROI would not be expected to affect the result. The convergence of Young's modulus E and the sum-squared difference ssd is given in figures 4(a) and (b) respectively, where the curves marked $\circ$ and $*$ represent the hard and soft layers respectively. It can be noted that, as the iteration number increases, E converges to the expected value while ssd approaches zero.

In order to investigate the error introduced by assuming a smaller value for Poisson's ratio in the solution of Young's modulus, as would be done when the actual value of ν is unknown, the simulated data were reanalysed using $\nu = 0.495$ in the iterative algorithm. The convergence of Young's modulus in the firmer layer ($E = 20$ kPa) is shown in figure 5 for

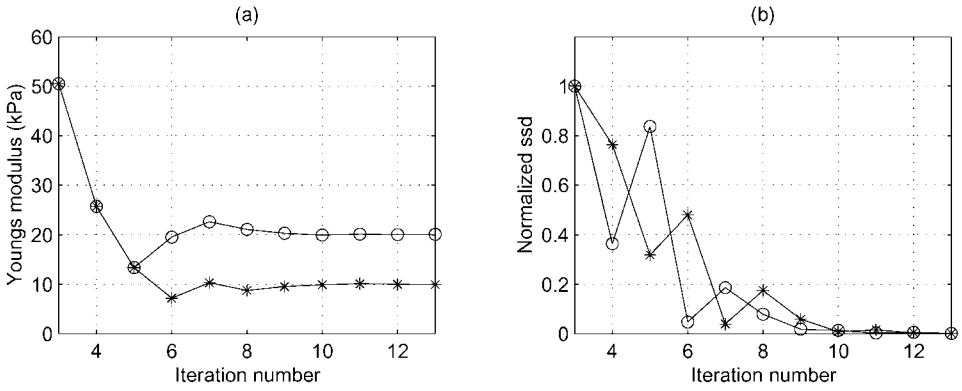

Figure 4. Convergence of results from FEM simulation data. The curves marked ∗ and ○ represent the soft and hard layers, respectively. (*a*) Convergence of Young's modulus. (*b*) Convergence of normalized ssd.

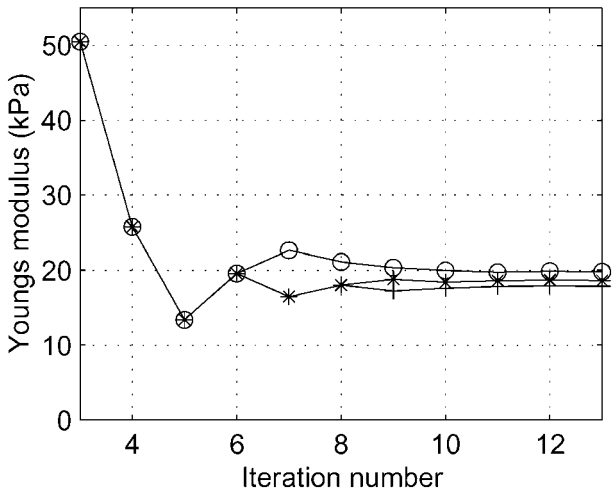

Figure 5. Sensitivity of Young's modulus to errors in the assumed Poisson's ratio for differing sizes of the ROI. The curves marked +, ∗ and ○ represent sizes of the ROI of 6 mm × 6 mm, 8 mm × 8 mm and 10 mm × 10 mm respectively.

different sizes of the ROI (6 mm × 6 mm, 8 mm × 8 mm and 10 mm × 10 mm). The estimation errors were 10.4%, 6.5% and 0.7% respectively, indicating increasing errors as the size of the ROI decreases.

As a test of the validity of the assumption of the undamped condition, simulations of motion in phantoms were generated using a variety of damping coefficients at four frequencies. Equation (10), which assumes no damping, was then used in the iterative solution algorithm to estimate Young's modulus from the FEM simulated data. The size of ROI was 10 mm × 10 mm. As illustrated in figure 6, the per cent error increases with increasing damping and vibration frequency, as expected.

The noise sensitivity of the algorithm was quantified by adding a Gaussian white noise source to the simulated displacements. The results are shown in figure 7 at various vibration frequencies: (*a*) 22.5 Hz, (*b*) 37.5 Hz, (*c*) 52.5 Hz and (*d*) 67.5 Hz. The mean of the Gaussian

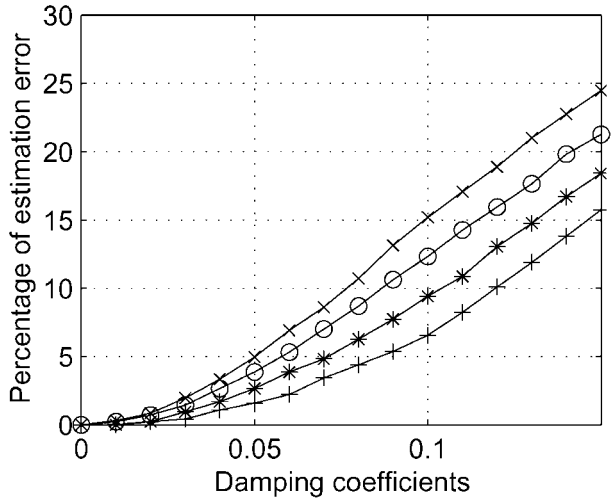

Figure 6. Sensitivity of Young's modulus to damping coefficients at different vibration frequencies. The size of the ROI is 10 mm × 10 mm. The curves marked +, ∗, ○ and *x* represent vibration frequencies of 22.5 Hz, 37.5 Hz, 52.5 Hz and 67.5 Hz respectively.

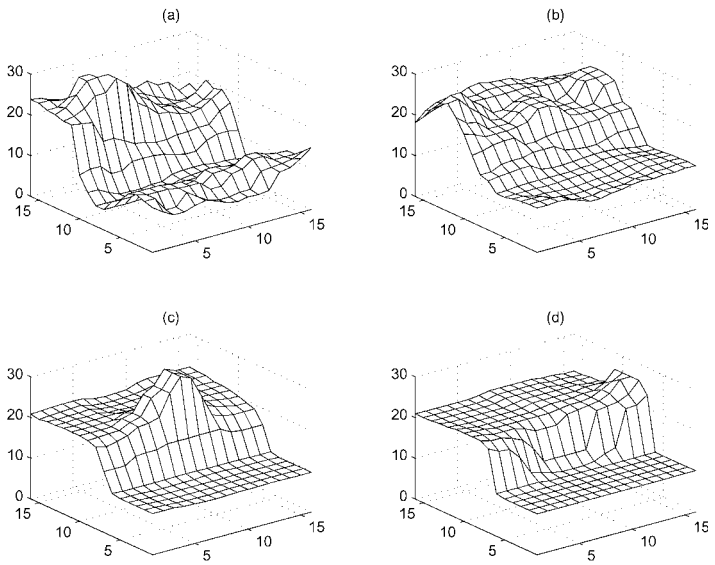

Figure 7. Distribution of Young's modulus in a two-layer structure estimated from simulated noisy displacements where the mean of Gaussian noise is 5% of the maximum displacement at vibration frequencies (*a*) 22.5 Hz, (*b*) 37.5 Hz, (*c*) 52.5 Hz and (*d*) 67.5 Hz.

noise was arbitrarily chosen to be 5% of the maximum displacement. A complete map of the Young's modulus was obtained by sliding a 10 mm × 10 mm ROI over the entire 2D domain. All of the results were smoothed using a median filter to remove spurious data points. It is noted that the noise performance improved with increasing vibration frequency in regions located entirely within a homogeneous layer. Because Young's modulus is related to the spatial derivatives of the underlying motion, increasing frequencies under conditions

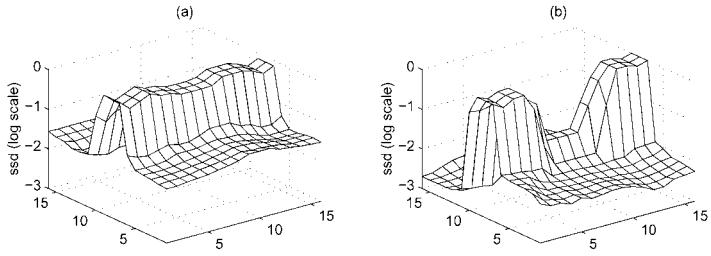

Figure 8. Distribution of log normalized ssd at vibration frequencies (*a*) 52.5 Hz and (*b*) 67.5 Hz, corresponding to the distribution of Young's modulus in figures 7(*b*) and (*d*) respectively.

of constant amplitude would be expected to result in an improved signal-to-noise ratio, as demonstrated by the results.

From figure 7, it is apparent at the higher vibration frequencies that, when the ROI is located within a homogeneous region, the estimated values of Young's modulus are accurate and stable. However, when the ROI crosses the boundary between two layers, the basic assumption that Young's modulus is constant within the ROI is violated and, hence, the results are unreliable. A confidence measurement can be established by observing the values of ssd. Figure 8 shows the distribution of the normalized ssd on a logarithmic scale. It is apparent that the ssd for regions where the assumption of homogeneity is violated is much larger than in homogeneous regions. It is also noted that the ssd decreases with increasing vibration frequency, suggesting a greater degree of confidence in the estimates obtained.

4. Experiments on tissue-mimicking phantoms

In our approach, reconstruction of the elastic properties of soft tissues involves the use of a mesh-based speckle tracking method to measure the vibrational motion from a B-scan image sequence. Young's modulus is then calculated from the measured vibrational motion using an iterative forward approach. Because both methods are mesh-based, the same mesh structure used for speckle tracking can be directly applied to elastic property reconstruction. These two steps can be integrated to provide a systems approach in which Young's modulus is estimated directly from ultrasonic B-scan data. In this section, ultrasound experiments on a homogeneous tissue-mimicking phantom and on a two-layer phantom were carried out to verify the overall approach.

The homogeneous phantom was composed of 800 g water, 77 g gelatin, 80 g glycerol, 8 g barium sulphate and 80 g formalin. The soft layer in the two-layer phantom was composed of 200 g water, 28 g gelatin, 40 g glycerol, 4 g barium sulphate and 40 g formalin. The hard layer was composed of 400 g water, 49 g gelatin, 40 g glycerol, 4 g barium sulphate and 40 g formalin. Phantom fabrication was based on Gao *et al* (1995). The shape of the phantoms is shown in figure 1 and the dimensions are 4 cm $\times$ 4 cm $\times$ 30 cm. In the experiment, a rigid bar measuring 16 cm in length and 0.6 $\times$ 0.6 cm in cross section was connected to a mini-shaker, and a horizontal vibration was applied to the left side surface. An ultrasound transducer was placed on the top surface, with the scan plane oriented perpendicular to the long axis of the phantom, and a GE Logiq 700 scanner was used to acquire cine B-mode data. The bottom and the right side surfaces were fixed. The frame rate of the scanner was 30 Hz. Two vibration frequencies of 67.5 Hz and 97.5 Hz were sequentially applied to each phantom. All of the experiments were carried out two days after the phantoms were made so as to ensure uniform consistency.

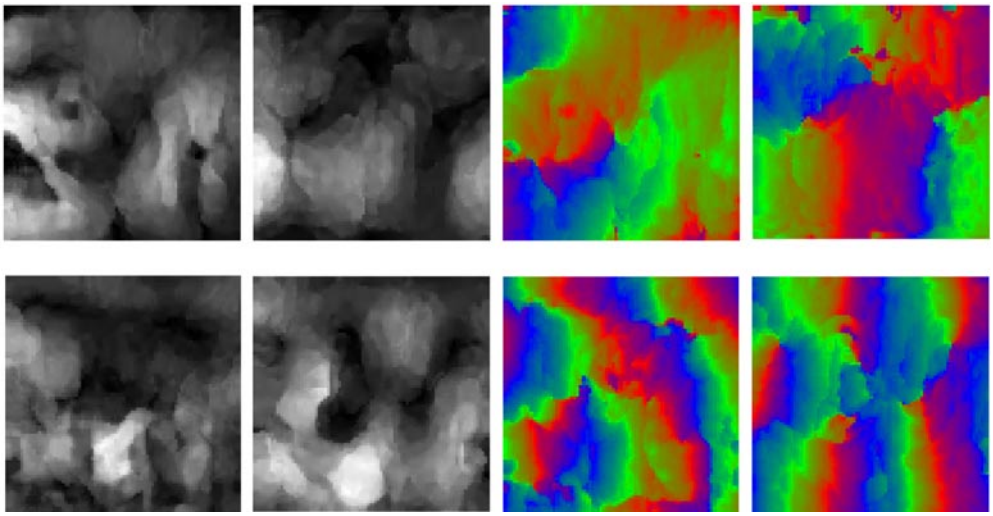

Figure 9. Images of vibration amplitude and phase estimated from four consecutive B-scan images of the homogeneous phantom where the vibration frequencies for the images in the first and second rows are 67.5 Hz and 97.5 Hz respectively. The four images from left to right are horizontal amplitude, vertical amplitude, horizontal phase and vertical phase respectively.

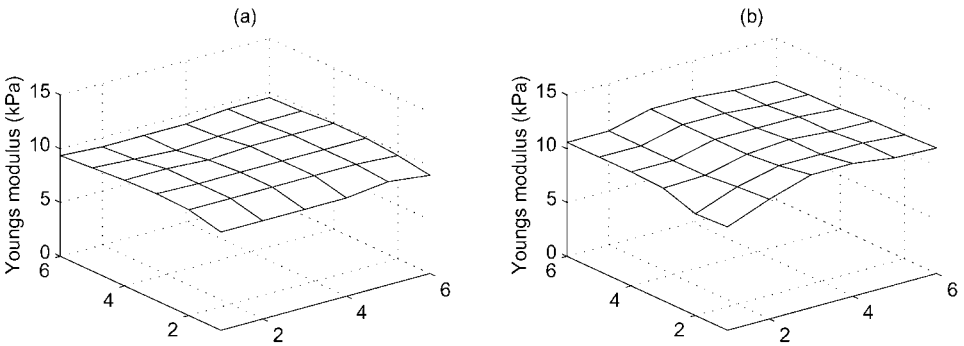

Figure 10. Distribution of Young's modulus in the homogeneous phantom estimated from the amplitude and phase at vibration frequencies of (*a*) 67.5 Hz and (*b*) 97.5 Hz.

In the experiments on the homogeneous phantom, four consecutive frames were chosen and the displacements between frames were estimated using the speckle tracking method. The vibration amplitude and phase were calculated using equations (12). The resulting images are shown in figure 9. Iterative forward elasticity estimation was performed on the calculated amplitude and phase data. The size of the ROI was 20 mm $\times$ 20 mm. The larger size was chosen for this preliminary experiment due to the higher than anticipated image noise. The distribution of the reconstructed Young's modulus was given in figure 10 at two different vibration frequencies, 67.5 Hz and 97.5 Hz.

To verify the accuracy of the estimates, the results were compared with independent measurements of Young's modulus made on a small circular cylindrical sample that had the same composition as the phantom. A simple load cell was used to statically compress the sample. Both the top and bottom surfaces were lubricated with vegetable oil to approximate a free slip boundary condition to create a uniform stress state within the sample. Young's

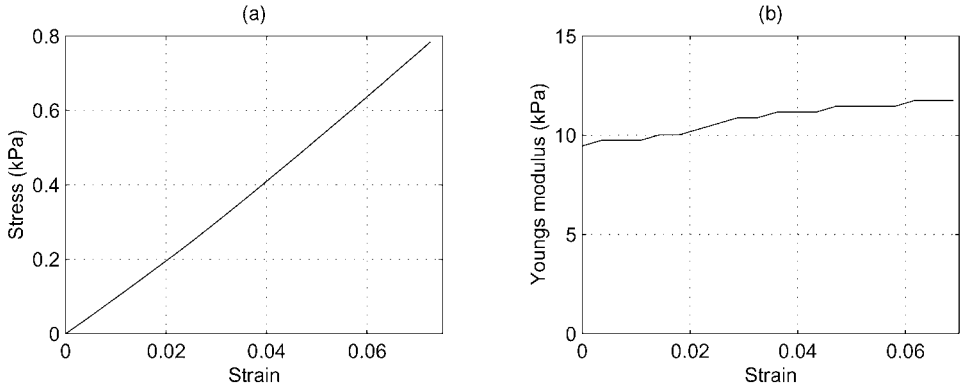

Figure 11. Results from static stress–strain measurements of a small circular cylindrical sample of the material used to construct the homogeneous phantom. (*a*) Stress–strain data. (*b*) Calculated Young's modulus.

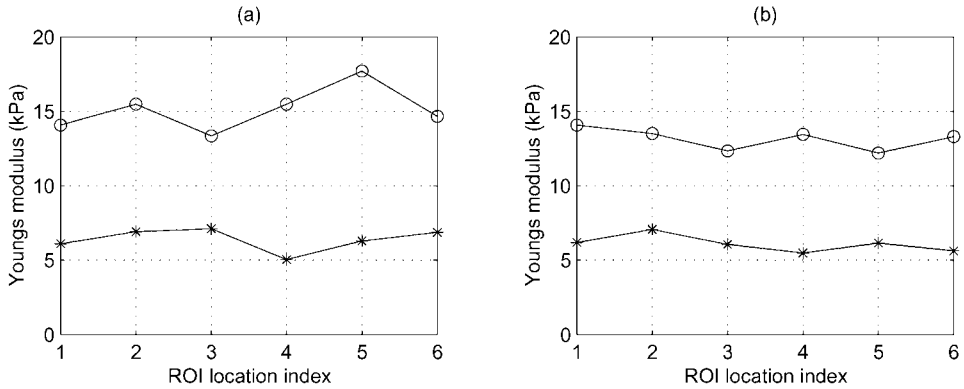

Figure 12. Young's modulus in each of the layers of a two-layer phantom, estimated from ultrasound experiments at vibration frequencies of (*a*) 67.5 Hz and (*b*) 97.5 Hz.

modulus values in figure 11(*b*) were calculated from the slope of the plot of stress versus strain in figure 11(*a*). The elastic response of the gel-based phantom is approximately linear and its Young's modulus is approximately 10 kPa, with a range of 9–12 kPa. The comparison of results in figures 10 and 11 shows that Young's modulus of the phantom estimated from the ultrasound B-scan differs from the value measured from the small sample by 10.4% at a strain of 2%.

The experiments were repeated using the two-layer phantom with the soft layer on the bottom and the hard layer on the top. A horizontal vibration was applied to the side surface of the hard layer. The size of the ROI was 25 mm $\times$ 15 mm. Because this is large relative to the thickness of each layer, the ROI was restricted to each homogeneous region and moved from left to right. The estimated Young's modulus is shown in figures 12(*a*) and (*b*) at vibration frequencies 67.5 Hz and 97.5 Hz respectively. The horizontal axis represents the horizontal position of the ROI within each layer. The Young's moduli of the soft and hard layers were also measured by independent measurements from small samples, as described for the homogeneous phantom, and the results are shown in figure 13. The Young's modulus from the ultrasound experiments agreed well with the results from the mechanical static measurements, differing by 11.9% in the soft layer and 10.5% in the hard layer at a strain of 2%.

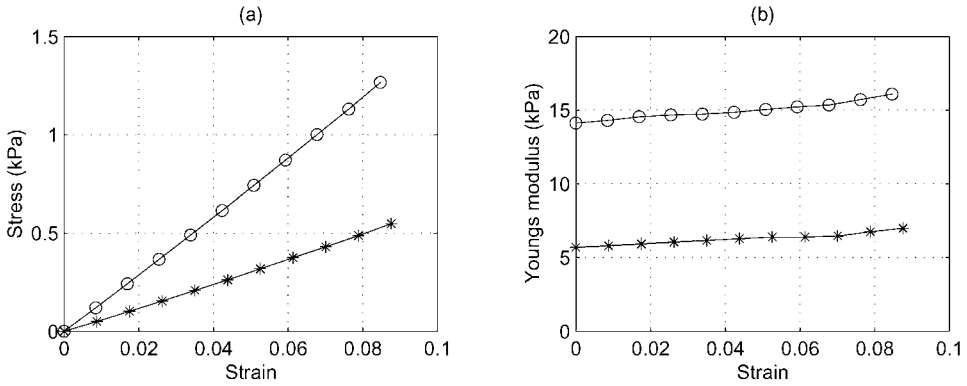

Figure 13. Experimental static stress–strain results from circular cylindrical samples of the materials used to construct the two-layer phantom. The curves marked ∗ and ○ represent the soft and hard layers respectively. (*a*) Stress–strain data. (*b*) Calculated Young's moduli.

5. Discussion

In this paper, we have presented a systems approach to the quantitative estimation of Young's modulus in soft tissue from sequences of vibrating ultrasound B-scan images. This was developed by integrating a mesh-based speckle tracking method with an iterative forward estimation approach to elastic reconstruction, both of which are based on FEM. Results from numerical simulations and initial measurements in phantoms demonstrate the viability of the approach, in which Young's modulus values can be obtained from as few as three consecutive B-mode ultrasound images. This work differs from previous methods in that complete elastic reconstruction is possible from a 2D vibration motion field (amplitude and phase) without the need for independent measurement of stress or for *a priori* knowledge of the elasticity at the boundaries. Skovoroda *et al* (1995, 1999) and Kallel and Bertrand (1996), in contrast measured one-dimensional displacements and estimated the relative elasticity assuming that the elasticity along the boundaries of the ROI is known.

Currently, our approach requires two basic assumptions. Firstly, a plane strain state is assumed so as to establish a 2D mechanical model, because most commercial ultrasound scanners can only acquire real-time data in two dimensions. Secondly, the soft tissues under investigation are assumed to be homogeneous, isotropic and linearly viscoelastic so that the Voigt model can be used to establish the constitutive equations. In reality, most soft tissues are three dimensional and tissue materials are usually anisotropic and nonlinear in their mechanical properties. It is often possible to restrict the geometry of the tissue under investigation, however, so that these criteria are approximately satisfied. For example, the human thigh when imaged in cross section and vibrated along its entire length can be considered to be transversely isotropic and in a plane strain state. The assumption of homogeneity is necessary in order to calculate a constant value of Young's modulus in each ROI. When the materials are inhomogeneous, the solution can become unstable and the results inaccurate, as demonstrated by the numerical simulation results in figure 7. Elastic property reconstruction in inhomogeneous media may thus require the use of image segmentation, possibly based on measured strain values. This will be investigated in our future work.

The error associated with the use of a predefined Poisson's ratio was found to be of significance only as the size of the ROI decreases below values that are currently practical. The error associated with non-zero damping, on the other hand, can be significant, particularly

as the frequency increases. This in effect places a limitation on the frequencies that can be used. Alternatively, equation (9) could be used to simultaneously solve for both Young's modulus and the damping coefficient, but with added complexity and the risk of instability. By alternating optimization of estimated values of Young's modulus and the damping ratio, we believe that we can reduce the effect of damping error within practical constraints, as we hope to demonstrate in future experiments.

The most significant limitation, however, rests with the accuracy of the speckle tracking method itself. The principal sources of error are decorrelation of the speckle patterns and quantization of the measured displacements. These do not conform to Gaussian statistics and, hence, the use of numerical simulations of data with superimposed Gaussian noise cannot accurately represent the speckle motion model. Theoretical models of speckle rotation and shearing for simulation that can accurately model decorrelation of speckle patterns are available in the literature (Kallel *et al* 1994, Maurice and Bertrand 1999). However, practical models of speckle for deformable vibrating media have not yet been developed. Because the elastic modulus is defined as the ratio of stress to strain, most methods of elastic property reconstruction involve at least the first-order derivatives of displacements, resulting in amplification of measurement error. Future efforts will focus on refining the model of speckle tracking error and its effect on elastic modulus estimation.

In our iterative forward method, the measured amplitude and phase values on the boundary of the ROI are used to calculate the values in the interior of the ROI, which are then compared with the measured values using ssd. The noise of the measured amplitude and phase values on the ROI boundaries will thus affect the accuracy of the estimated Young's modulus. The vibration frequency is also an important factor that affects the accuracy of elasticity estimation. The results in figure 7 clearly demonstrate that elasticity estimation is less sensitive to noise with increasing vibration frequency. This results from larger spatial gradients and reduced noise. However, in real situations, higher frequencies result in decreased amplitudes and increased quantization error, not to mention damping error. The size of the ROI is another important factor. The larger the size, the more accurate the results, but the poorer the spatial resolution. Because most methods of displacement estimation are subject to image noise, the sensitivity to noise is a very important factor that will ultimately determine the practical implementation of elastic property reconstruction algorithms in real situations.

Our future work will seek to improve the accuracy of the mesh-based speckle tracking algorithm and to optimize the vibration frequency and the size of the ROI so as to provide the best possible balance between image resolution and noise. The method will be further verified in phantoms with more complex geometry and in human soft tissues.

Acknowledgments

The authors gratefully acknowledge the support of General Electric for the provision of the GE Logiq 700 ultrasound scanner and, in particular, for the assistance of Drs Kai Thomenius and Anne Hall. This project was supported by NIH grant 1R01HD35638.

References

Catheline S, Wu F and Fink M 1999 A solution to diffraction biases in sonoelastography: the acoustic impulse technique *J. Acoust. Soc. Am.* **105** 2941–50

Cook R D, Malkus D S and Plesha M E 1989 *Concepts and Application of Finite Element Analysis* (New York: Wiley) pp 368–70

Gao L, Parker K J, Alam S K and Lerner R M 1995 Sonoelasticity imaging: theory and experimental verification *J. Acoust. Soc. Am.* **97** 3875–86

Hein I A and O'Brien W D 1993 Current time-domain methods for assessing tissue motion by analysis from reflected ultrasound echoes—a review *IEEE Trans. Ultrason. Ferroelectr. Freq. Control* **40** 84–102

Kallel F and Bertrand M 1996 Tissue elasticity reconstruction using linear perturbation method *IEEE Trans. Med. Imaging* **15** 299–313

Kallel F, Bertrand M and Meunier J 1994 Speckle motion artifact under tissue rotation *IEEE Trans. Ultrason. Ferroelectr. Freq. Control* **41** 105–22

Krouskop T A, Dougherty D R and Levinson S F 1987 A pulsed Doppler ultrasonic system for making non-invasive measurements of the mechanical properties of soft tissue *J. Rehabil. Res. Dev.* **24** 1–8

Krouskop T A, Wheeler T M, Kallel F, Garra B S and Hall T 1998 Elastic modulus of breast and prostate tissues under compression *Ultrason. Imaging* **20** 260–74

Lerner R M, Huang S R and Parker K J 1990 Sonoelasticity images derived from ultrasound signals in mechanically vibrated tissue *Ultrasound Med. Biol.* **16** 231–9

Levinson S F, Shinagawa M and Sato T 1995 Sonoelastic determination of human skeletal muscle elasticity *J. Biomech.* **28** 1145–54

Maurice R L and Bertrand M 1999 Speckle-motion artifact under tissue shearing *IEEE Trans. Ultrason. Ferroelectr. Freq. Control* **46** 584–94

Muthupillai R, Lomas D J, Rossman P J, Greenleaf J F, Manduca A and Ehman L 1995 Magnetic resonance elastography by direct visualization of propagating acoustic strain waves *Science* **290** 1854–7

O'Donnell M, Skovoroda A R, Shapo B M and Emelianov S Y 1994 Internal displacement and strain imaging using ultrasonic speckle tracking *IEEE Trans. Ultrason. Ferroelectr. Freq. Control* **41** 314–25

Ophir J, Cespedes I, Ponnekanti H, Yazdi Y and Li X 1991 Elastography: a quantitative method for imaging the elasticity of biological tissue *Ultrason. Imaging* **13** 111–34

Ophir J, Kallel F, Varghese T, Bertrand M, Cespedes I and Ponnekanti H 1997 Elastography: a systems approach *Int. J. Imaging Syst. Technol.* **8** 89–103

Parker K J, Fu D, Gracewski S M, Yeung F and Levinson S F 1998 Vibration sonoelastography and the detectability of lesions *Ultrasound Med. Biol.* **24** 1437–47

Parker K J, Huang S R and Lerner R M 1990 Tissue response to mechanical vibrations for sonoelasticity imaging *Ultrasound Med. Biol.* **16** 241–6

Radmacher M 1997 Measuring the elastic properties of biological samples with the AFM *IEEE Eng. Med. Biol.* **16** 47–57

Romano A J, Shirron J J and Bucaro J A 1998 On the noninvasive determination of material parameters from knowledge of elastic displacements: theory and numerical simulation *IEEE Trans. Ultrason. Ferroelectr. Freq. Control* **45** 751–9

Skovoroda A R, Emelianov S Y and O'Donnell M 1995 Tissue elasticity reconstruction based on ultrasonic displacement and strain images *IEEE Trans. Ultrason. Ferroelectr. Freq. Control* **42** 747–65

Skovoroda A R, Lubinski M A, Emelianov S Y and O'Donnell M 1999 Reconstructive elasticity imaging for large deformation *IEEE Trans. Ultrason. Ferroelectr. Freq. Control* **46** 523–35

Sumi C, Suzuki A and Nakayama K 1995 Estimation of shear modulus distribution of soft tissue from strain distribution *IEEE Trans. Biomed. Eng.* **42** 193–202

Yamakoshi Y, Sato J and Sato T 1990 Ultrasonic imaging internal vibration of soft tissue under forced vibration *IEEE Trans. Ultrason. Ferroelectr. Freq. Control* **37** 45–53

Yeung F, Levinson S F, Fu D and Parker K J 1998 Feature-adaptive motion tracking of ultrasound image sequences using a deformable mesh *IEEE Trans. Med. Imaging* **17** 945–56